

RESEARCH ARTICLE

## Magnetic/pH-sensitive nanocomposite hydrogel based carboxymethyl cellulose-g-polyacrylamide/montmorillonite for colon targeted drug deliver

Gholamreza Mahdavinia<sup>1</sup>; Ali Afzali<sup>2</sup>; Hossein Etemadi<sup>1\*</sup>; Hossein Hosseinzadeh<sup>2</sup>

<sup>1</sup>Laboratory for Polymer Research, Department of Chemistry, Faculty of Science, University of Maragheh, Maragheh, Iran

<sup>2</sup>Department of Chemistry, University of Payame Noor, West Azerbaijan, Miandoab, Iran

### ARTICLE INFO

#### Article History:

Received 12 February 2017

Accepted 12 May 2017

Published 14 May 2017

#### Keywords:

Carboxymethyl cellulose

Magnetic montmorillonite

Drug release

Swelling

Diclofenac sodium

### ABSTRACT

**Objective(s):** The main aim of current research was to develop a novel magnetically responsive hydrogel by radical polymerization of carboxymethyl cellulose (CMC) on acryl amide (Am) using N,N'-methylene bis acrylamide (MBA) as a crosslinking agent, potassium persulfate (KPS) as a free radical initiator, and magnetic montmorillonite (mMT) nanoclay as nano-filler.

**Methods:** The new product (CMC-g-Am/mMT) was characterized by FT-IR, XRD, TEM, SEM, and VSM techniques. Drug loading and release efficiency were evaluated by Diclofenac Sodium (DS) as a model drug.

**Results:** SEM results demonstrated that magnetic nanoclay (mMT) can cause a rough morphology. Transmission electron microscopy (TEM) indicated the formation of MNPs into the montmorillonite clay structure with the final average particle size of around 100 nm. Furthermore, according to the in vitro drug release profiles, the maximum cumulative release was around 79% at pH=7.4 under applied magnetic field.

**Conclusions:** The results indicate that the prepared CMC-g-Am/mMT platform can be used for delivery of drugs to the colon by applying an external magnetic field.

#### How to cite this article:

Mahdavinia Gh, Afzali A, Etemadi H, Hosseinzadeh H, Magnetic/pH-sensitive nanocomposite hydrogel based carboxymethyl cellulose-g-polyacrylamide/montmorillonite for colon targeted drug delivery. *Nanomed Res J*, 2017; 2(2):111-122. DOI: 10.22034/nmrj.2017.58964.1058

## INTRODUCTION

Over the past few years, particular interest has been paid towards the fabrication of new drug delivery systems (DDS) to specifically deliver the therapeutic agents to target sites [1-2]. This technology offers great advantages over conventional DDS such as low toxicity, wide therapeutic window, minimized side effects, ideal drug efficacy and releasing drugs in a sustained rate [3]. Magnetic targeting can be achieved through the introduction of magnetic nanoparticles into the drug-carrier matrices [4]. Magnetic nanoparticles have been of considerable interest for their practical biomedical applications. Particularly,

\* Corresponding Author Email: [hosseinetemadi39@yahoo.com](mailto:hosseinetemadi39@yahoo.com)

ultrafine size and highly crystalline magnetic iron oxide nanoparticles (MNPs) is garnering substantial attention because of possessing superior characteristics like superparamagnetism, high surface-to-volume ratio, high field saturation and biocompatibility [5-6]. However, the main challenge is self-aggregation of these particles because of their high surface energy and strong magnetic dipole-dipole interactions. Most importantly, for biomedical applications, it is of fundamental importance modifying the surface of nanoparticles with water-soluble and specific functionalized groups to enable conjugation of the drug [7]. Therefore developing well-defined

strategies for functionalization of MNPs with well-considered nanostructures is in great demand. Of all the available materials, non-toxic polysaccharide based hydrogels such as chitosan, alginate, Carrageenan, starch, gelatin and carboxy methyl cellulose is increasingly being used as one of the most significant matrices in new biomedicine applications [8-10]. Among all the polysaccharides, carboxymethyl cellulose (CMC) is the most widely used and easily available cellulose ether today. It is biocompatible, biodegradable, hydrophilic, non-toxic, and very cheap [11-12]. Owing to a number of sodium carboxymethyl ( $\text{CH}_2\text{COONa}$ ) and hydroxyl (-OH-) groups promote water solubility and high chemical stability [13]. It has been used in various drug delivery applications especially as bioadhesive material, for nasal and buccal drug delivery systems [14]. A crucial perspective for application of hydrogels as drug delivery systems is the degree of swelling. However, a single problem associated with use of conventional hydrogels in drug delivery purposes is weak and fragile architecture because of the large proportion of water penetrated in their structure [15]. To address this problem and enhance stability, one strategy is based on the use of nanoclays [16]. In order to modify drug release, a fascinating approach is to use polymer/layered silicate nanocomposites. These hybrid materials carry out specific functions such as modifying drug delivery patterns, improving drug dissolution and increasing drug stability [17]. Among layered silicate materials, considerable attention has been drawn towards montmorillonite (MT) nanoclay because of possessing substantial properties such as large specific surface area, rheology, chemical inertness, bioadhesion, high cation exchange capacity and good absorbance ability [18]. Additionally, MT has also been found to be non-toxic by histopathological, hematological, and biochemical investigations in rat models [19]. These inherent advantages make MT-Clay mineral to be used successfully as vehicles for delivery of drug molecules. Some shiny examples include intercalation of donepezil in montmorillonite for Alzheimer disease [20]. Intercalation of 5- fluorouracil with MT as a drug vector [21] and encapsulation of paclitaxel in Poly (D, L-lactide-co-glycolide)/ MT for breast cancer chemotherapy [22]. The novelty of present study was development of dual magnetic/pH sensitive

hydrogel composed of carboxymethyl cellulose-g-acrylamide in the presence of montmorillonite nanoclay with the ultimate goal of the medically applicable device for colon specific drug delivery through oral administration.

## MATERIALS AND METHODS

### *Chemicals and Reagents*

Sodium carboxymethyl cellulose (NaCMC) and diclofenac sodium were purchased from Sigma-Aldrich (St. Louis, USA). Natural sodium-montmorillonite (sodium Cloisite, Na-MT) as a clay with cation exchange capacity of 92 meq/100 g of clay was provided by Southern Clay Products (USA). Acrylamide was purchased from Nalco Chemical Co. (Netherlands) and used after recrystallization from acetone. N, N-methylenebisacrylamide and ammonium persulfate were purchased from Merck (Germany). All other chemicals were analytical grade and used without any purification.

### *Synthesis of magnetic montmorillonite (mMT)*

The magnetic montmorillonite (mMT) was manufactured according to our previous work [23]. 3g of sodium montmorillonite was dispersed in 200 mL distilled water and stirred for overnight. The dispersed clay was then sonicated for 20 min under the induced frequency of 60 kHz. Afterward, the certain amount of  $\text{Fe}^{3+}/\text{Fe}^{2+}$  with a molar ratio of 1:2 were dissolved in distilled water with vigorous mechanical stirring for 90 min. Two solutions with the ratio reported by Wu et al were mixed and allowed to stir for 30 min [24]. Then, the ammonia (3M) was added dropwise into the above solutions and allowed to reach the pH of 11. The prepared mMT was stirred at 70°C for 2h and consequently cooled to ambient temperature. The solution was centrifuged and washed with distilled water several times. Finally, the mMT was separated by a magnet and the volume of solution was adjusted to 80 mL.

### *Preparation of PAm grafted CMC intercalated*

mMT (CMC-g-Am/mMT) CMC-g-Am/mMT hydrogels were synthesized via grafting of Am onto CMC using MBA as a crosslinking agent, KPS, as a free radical initiator, and mMT nanoclay as nano-filler. In the undertaken protocol, 1 g of CMC was poured in distilled water and was stirred at ambient temperature for 90 min. 3g of Am monomer and 0.10g of MBA (dissolved in 2 mL of distilled water)

were added into the above solution. The mixture was stirred for 1 h and subsequently 0.10g of the APS was added to the reactor while stirring. After that, mMT solution of different volumes (0, 10 and 15 mL) was added to the reaction media and sonicated for 10min. The resultant were collected and washed with excess water, dried at ambient temperature for constant weight. The as-prepared resultants were coded as CMC-g-Am, CMC-g-Am/mMT1 and CMC-g-Am/mMT2.

#### Water uptake measurements

To study water absorbency (WA), two different sets of experiments were performed which include dynamic swelling measurement at simulated intestinal fluid (SIF) (phosphate buffer solution (PBS, pH 7.4): 8g NaCl, 0.2g KCl, 1.44 Na<sub>2</sub>HPO<sub>4</sub>, 0.24 KH<sub>2</sub>PO<sub>4</sub>, 1L H<sub>2</sub>O) and simulated gastric fluid (SGF) (hydrochloric acid buffer solution (HBS, pH 1.2): 0.15M HCl, 0.05M KCl) and kinetic swelling measurement in distilled water. For swelling measurements, the dry hydrogels (~0.2g) were placed in media and kept at a constant temperature, 20±0.5°C. Swollen samples were periodically removed, weighted and the water absorbency was measured according to Eq. 1:

$$WA(g/g) = \frac{W_s - W_d}{W_d} \quad (1)$$

Where  $W_s$  and  $W_d$  are the weights of the samples swollen in buffers and in a dry state, respectively. The all swelling data were repeated three times and the mean values were shown in graphs (mean±S.D. n=3).

Diclofenac sodium (DS) was used as a model drug. For loading DS molecules, 100mg of hydrogels were left to soak in 3mL of an aqueous solution of DS (500mg/L) at room temperature for 48h. After this time, samples were withdrawn from drug solution and washed with distilled water to remove the adsorbed drug on the surface of hydrogels, and the liquid was taken to be analyzed by UV-vis absorption spectroscopy by monitoring the absorbance changes at  $\lambda_{max}=276\text{nm}$ . The amount of DS loaded by the hydrogels was calculated by the following Eq. 2:

$$\text{Encapsulation Efficiency (EE\%)} = \frac{C_0 - C_t}{C_0} \times 100 \quad (2)$$

Where,  $C_0$  is the initial concentration of DS in the

solution (mg/L) and  $C_t$  is the concentration of DS remained in the media (mg/L)

#### In vitro drug release

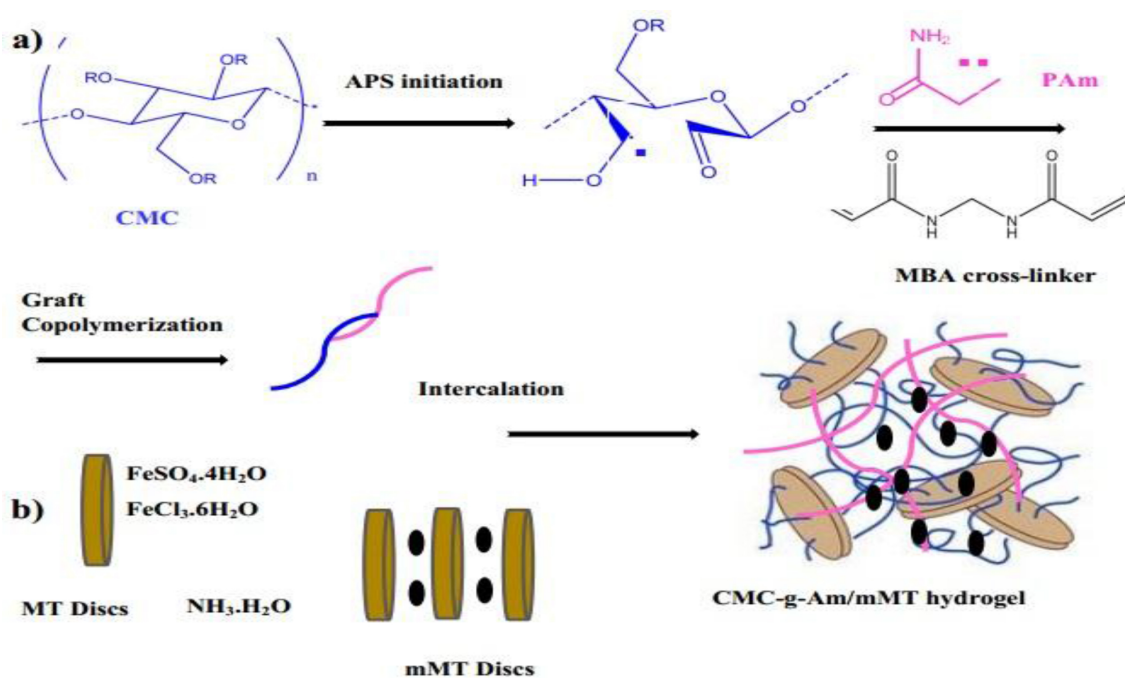
The release profile of Diclofenac sodium (DS) loaded hydrogels was evaluated at different pHs (1.2 and 7.4) and magnetic field (100 and 300 G). In each drug release experiment, certain amount of drug loaded hydrogels was sealed into 20 mL buffered solutions with pH 1.2 and 7.4. The release medium (5mL) was withdrawn at predetermined time intervals and the amount of released drug was quantified spectrophotometrically at  $\lambda_{max}=276\text{nm}$ . After each measurement, the withdrawn medium was replaced by 5 mL of fresh buffered solution. The cumulative release (R, %) of drug from samples was calculated according to Eq. 3:

$$R(\%) = \frac{M_t}{M_\infty} \times 100 \quad (3)$$

Where  $M_t$  and  $M_\infty$  are the drug released at time  $t$  and initial loaded drug content, respectively. The all releasing data were repeated 3 times and the mean values were shown in graphs (mean±SD. n=3). An external alternative magnetic field (AMF) apparatus (Electromagnet Type E, Newport Instruments, England) was also employed to monitor the magnetically drug release in phosphate buffer pH=7.4. Magnetic field frequency of 350 kHz and the strength of magnetic fields (100 and 300G) were set by adjusting the voltage of the equipment. The hydrogels were immersed in 10 mL of buffered solution with pH 7.4 and kept between magnetic poles for 180 min. The supernatant was used to calculate the amount of released drug during 180 min.

#### Structural characterization

The surface morphology of hydrogels was observed by field-emission scanning electron microscope (FESEM; NanoSEM 630, NOVA, USA) equipped with an energy-dispersive X-ray analysis system (EDXA). X-ray diffraction (XRD) pattern of the hydrogels was recorded on a Siemens D-500 X-ray diffractometer (ESCALAB220i-XL, VG Scientific, UK) with Cu K $\alpha$  radiation (30kV, 30mA) in the  $2\theta$  range from 2 to 80°. The magnetic properties of the products were measured on a Lake Shore 7400 vibrating sample magnetometer (VSM, Model 7400, Lakeshore Company, USA).



Scheme 1: Schematic route for the synthesis of CMC-g-Am/mMT hydrogel

Transmission electron microscopy (TEM) images were taken with a Zeiss EM 900 TEM (Zeiss SMT, Oberkochen, Germany) at 80 kV. FT-IR Spectra were recorded between 400–4000 $\text{cm}^{-1}$  by a Bruker 113V FT-IR spectrometer. (USA). Ultraviolet-visible (UV-Vis) absorption spectra were measured on an UV-VIS-NIR spectrophotometer (Shimadzu UV-Vis 3600, Japan).

## RESULTS AND DISCUSSION

### Synthesis and characterization

The magnetic nanocomposite hydrogels (CMC-g-Am/mMT) were prepared by the methodology reported by Mohapatra [25]. Schematic route for the synthesis of CMC-g-Am/mMT hydrogel was prepared (Scheme 1). In this protocol, firstly the MNPs were prepared in the presence of montmorillonite clay (mMT). The magnetic nanoclay was then modified by CMC-g-Am through in situ graft copolymerization of Acrylamide by using KPS as a free radical initiator, and MBA as a crosslinking agent.

### FTIR and XRD analysis

The FT-IR spectroscopy was carried out to confirm the chemical structures of synthesized hydrogels. Fig. 1a represents the spectra of CMC,

CMC-g-Am, MT and mMT samples respectively. The FT-IR spectrum of pure CMC presents the broad absorption band at 3445 $\text{cm}^{-1}$  indicating the stretching frequency of the -OH groups. The bands at 2932 and 1065 $\text{cm}^{-1}$  represent the stretching vibration of C-H and C-O bonds, respectively. In the FT-IR spectrum of CMC-g-Am the presence of amide groups is confirmed by appeared bands at 3209 and 1611 $\text{cm}^{-1}$  correspondent to the stretching and bending of N-H in amide groups. According to the MT spectrum, the characteristic vibration bands of the clay appear at 3634 $\text{cm}^{-1}$  (-OH stretch of the lattice hydroxyl), 3448 $\text{cm}^{-1}$  (-OH stretch from free  $\text{H}_2\text{O}$ ), 1643 $\text{cm}^{-1}$  (-OH bending) 1041 $\text{cm}^{-1}$  (Si-O stretch) and 522 and 460 $\text{cm}^{-1}$  (Si-O-Al and Si-O-Si bending vibrations) respectively. The FT-IR spectra of mMT demonstrated that by the introduction of MNPs into clay matrix due to van der Waals interactions between the oxygen groups of MT and MNPs, Fe-O bending vibrations of MNPs was shifted to low wave numbers. The bands between 436 $\text{cm}^{-1}$  and 615 $\text{cm}^{-1}$  were ascribed to Fe-O stretching vibration of MNPs which may be due to the overlapping of Si-O and Al-OH [26]. The crystalline structures and phase purities of as-synthesized hydrogels were studied by XRD patterns. The XRD patterns of pristine

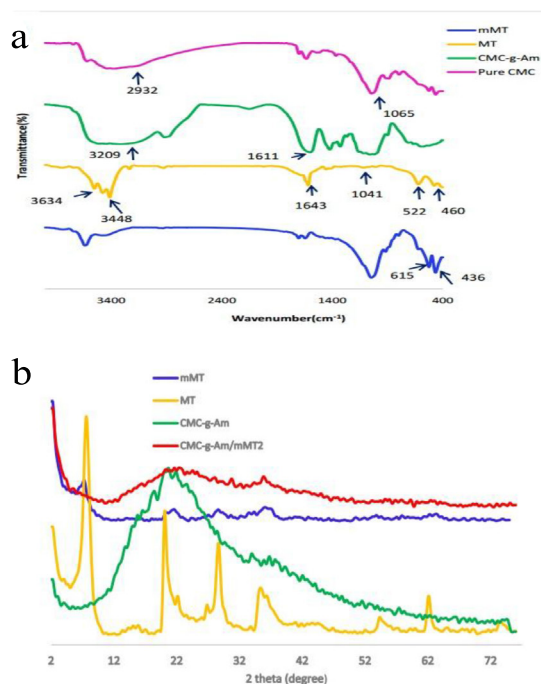


Fig. 1. (a) FT-IR Spectrum of pure CMC, CMC-g-Am, MT and mMT. (b) XRD patterns of pure MT, mMT, CMC-g-Am, and CMC-g-Am/mMT1 hydrogels

montmorillonite (MT) magnetic montmorillonite (mMT), CMC-g-Am, CMC-g-Am/mMT1 and CMC-g-Am/mMT2 hydrogels were shown in Fig. 1b. In the spectrum of neat MT a diffractive peak at  $2\theta=7.6^\circ$  was observed which corresponds to the layered MT clay with d-spacing of 11.61 Å. Compared to the XRD pattern of MT, the characteristic peak at  $2\theta=7.6^\circ$  was disappeared in the XRD pattern of mMT indicating the exfoliation of MT. Notably, during the synthesis of magnetic montmorillonite, the cation exchange can occur between  $\text{Na}^+$  and  $\text{Fe}^{3+}$  (or  $\text{Fe}^{2+}$ ), and the synthesized MNPs can be located between clay sheets as well as on the surface of clay [27]. The six characteristic peaks of MNPs appeared at  $2\theta$  about  $30.4^\circ$ ,  $35.4^\circ$ ,  $43.5^\circ$ ,  $53.3^\circ$ ,  $57.4^\circ$ , and  $63.2^\circ$  illustrating the corresponding indices (220), (311), (400), (422), (511), and (440), respectively. The interplaner distances were calculated according to Bragg's equation and found to be  $2.91\text{ \AA}$  ( $2\theta=30.4^\circ$ ),  $2.523\text{ \AA}$  ( $2\theta=35.4^\circ$ ),  $2.086\text{ \AA}$  ( $2\theta=43.5^\circ$ ),  $1.706\text{ \AA}$  ( $2\theta=53.3^\circ$ ),  $1.606\text{ \AA}$  ( $2\theta=57.4^\circ$ ), and  $1.47\text{ \AA}$  ( $2\theta=63.2^\circ$ ). The results are in accord with the database in JCPDS file (PDF No. 65-3107) indicating the formation of highly crystalline and pure magnetite nanoparticles

with spinel structure. The broad peak at  $2\theta=7-17^\circ$  may be attributed to the silicate composition of MT [28]. The XRD patterns of CMC-g-Am, CMC-g-Am/mMT1 and CMC-g-Am/mMT2 hydrogels are depicted in Fig. 1b as well. The CMC-g-Am hydrogel displayed a common broad diffraction peak at ( $2\theta=20^\circ$ ) illustrating the amorphous nature of PAM and the carbohydrate [29]. The same diffraction peak with low intense was observed in nanocomposite hydrogel containing magnetic nanoclay, CMC-g-Am/mMT1 and CMC-g-Am/mMT2 suggesting that the clay layers are fully or partially exfoliated.

#### SEM-EDX studies

Field emission scanning electron microscopy (FE-SEM) coupled with energy dispersive spectroscopy (EDS) offers a semiquantitative elemental analysis of the surface of materials. At the first step, the surface morphology of dried hydrogels was exploited by FESEM technique and micrographs were shown in the Fig. 2a-c.

From SEM images, it was found that the quantity of (mMT) plays a drastic role in changing the morphology of the products. The free magnetic-clay hydrogel (CMC-g-Am) showed a relatively smooth and tight surface (Fig.2a). Interestingly incorporation of magnetic montmorillonite (mMT) significantly affected the morphology of hydrogels. As could be seen from Fig. 2b-c a rough structure was obtained for magnetic hydrogels, confirming the hydrogel intercalation in interlayer galleries of mMT. This observation is similar to our previous works using Na-MMT as nanoclay [24]. Furthermore, the presence of magnetic nanoclay (mMT) in composition of hydrogel was confirmed by EDS spectra. EDS analysis on the other hand confirmed the formation of MNPs and MT by peak areas of (Fe and O) and (Na, Si, S) atoms in the hydrogel matrix. The EDS of CMC-g-Am, CMC-g-Am/mMT1 and CMC-g-Am/mMT2 was shown in Fig. 2a-c respectively. The characteristic peaks of Fe and Si appeared in the EDS spectra of both magnetic hydrogels. According to data, the content of Fe and Si in CMC-g-Am/mMT1 was obtained 2.38 and 12.73 %wt respectively. The content of Fe and Si in CMC-g-Am/mMT2 was 3.56 and 28.34 % wt respectively. This observation was in agreement with initial mMT used in synthesis process [24].

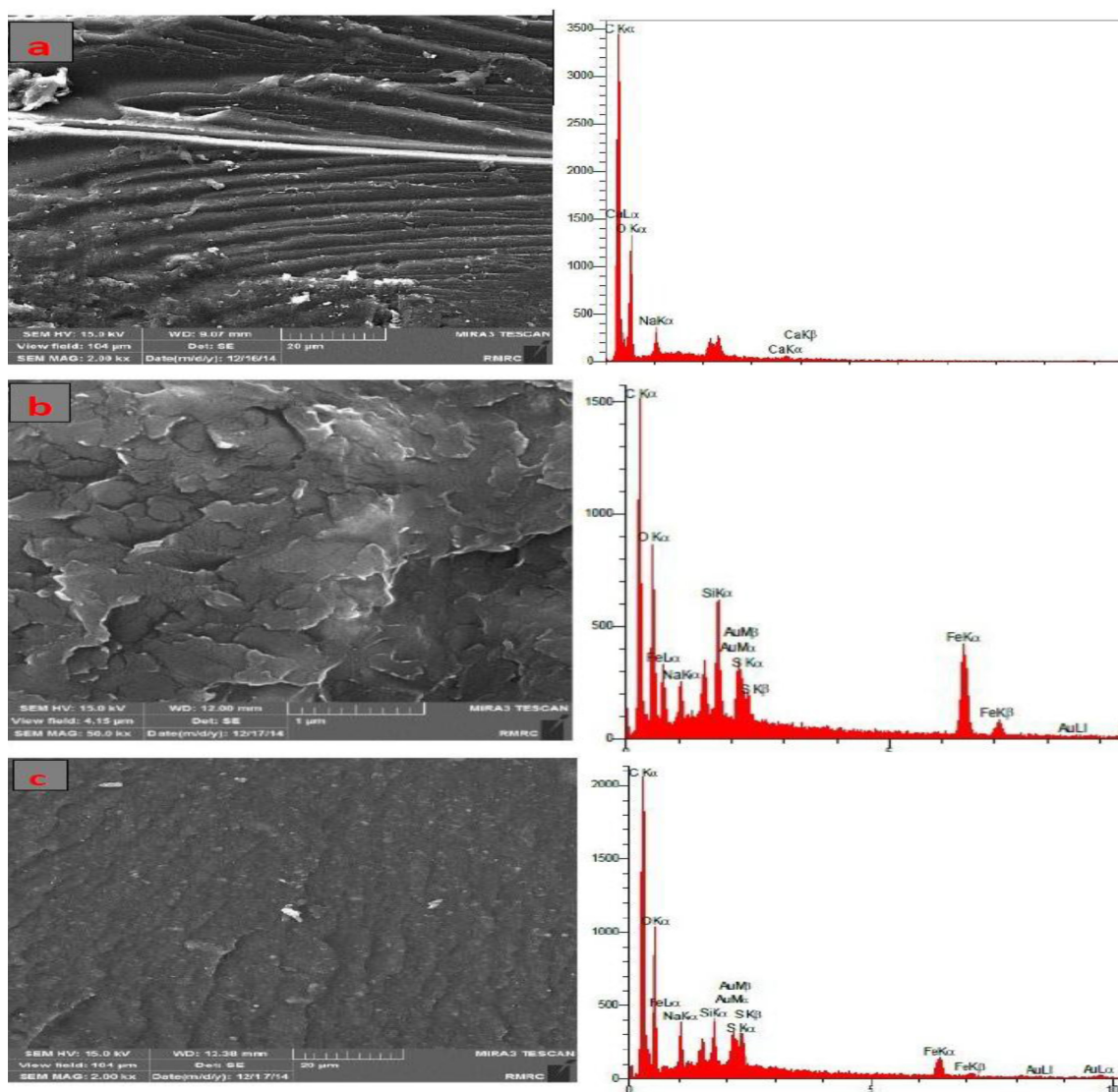


Fig. 2. SEM/EDS images of (a) CMC-g-Am, (b) CMC-g-Am/mMT1 and (c) CMC-g-Am/mMT2 hydrogels

#### VSM and TEM studies

The hysteresis loops of CMC-g-Am/mMT hydrogel were measured by VSM technique between  $\pm 9$  kOe at 298 K shown in Fig.3a. The magnetization curves illustrated that both CMC-g-Am/mMT1 and CMC-g-Am/mMT2 hydrogels were superparamagnetic with no coercivity at room temperature. The saturation magnetization values for CMC-g-Am/mMT1 and CMC-g-Am/mMT2 hydrogels were 0.55 and 0.72 emu g<sup>-1</sup>, respectively indicating that magnetic intensity of the CMC-g-Am/mMT hydrogel can be tuned by altering the weight ratio of MNPs [30]. Meanwhile,

TEM image of CMC-g-Am/mMT2 depicted the presence of the nano-network architecture, shown in Fig.3b. The MNPs were found to be embedded with clay plates where no single nanoparticles were detected inside the hydrogel network.

#### Water uptake

Fig.4a represents the dynamic swelling behavior of magnetic hydrogels in distilled water. Obviously, the swelling degree of hydrogels exhibited a systematic trend in accordance with composition, in which the water uptake decreases with increased ratio of magnetic nanoclay. The swelling capacity of magnetic hydrogels was obtained lower than

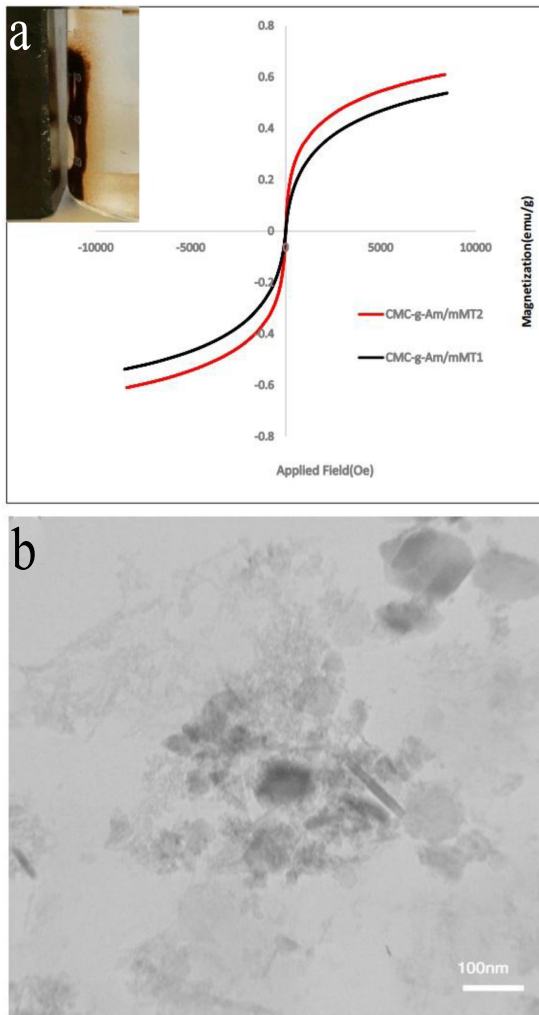


Fig. 3. (a) The hysteresis loops of CMC-g-Am/mMT1 and CMC-g-Am/mMT2 hydrogels versus applied magnetic field. (b) TEM image of CMC-g-Am/mMT2.

the free magnetic-clay hydrogels Maximum and minimum swelling capacity was obtained for free free-magnetic-clay CMC-g-Am and CMC-g-Am/MT2 hydrogels, respectively. This decrement in water absorbency can be attributed to the presence of MNPs and MT nanoclay as well. From one hand, the introduction of MNPs will cause (a) decrease in the ratio of hydrophilic and anionic functional groups and (b) the interaction between MNPs and polymeric chains can result in more crosslink points and thereby decrease in swelling capacity [31]. On the other hand, by increasing the contents of MT the swelling ratios of hydrogels gradually decreased. Two phenomenons are

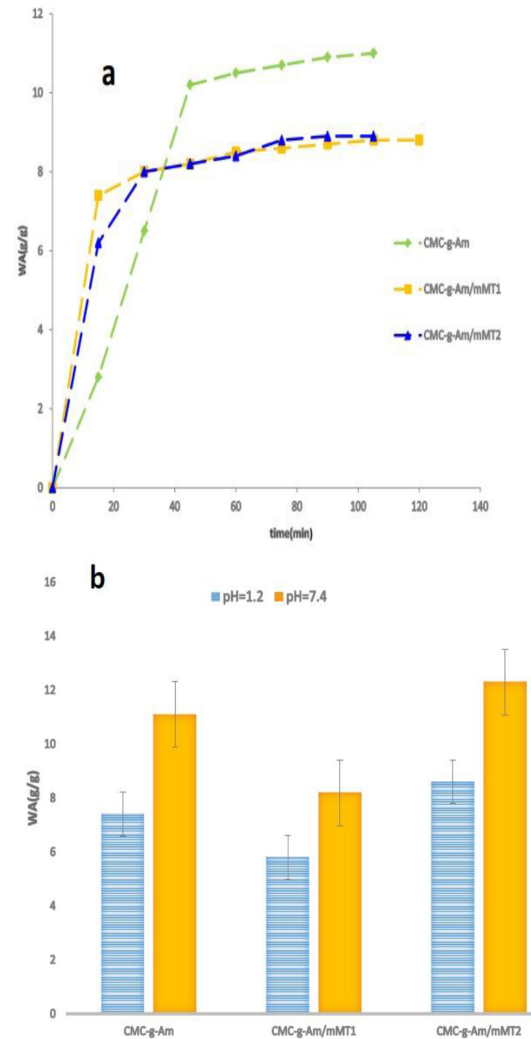


Fig. 4. (a) Swelling kinetic of hydrogels in distilled water. (b) Effect of pH on swelling degree of hydrogels

involved here. Firstly, increasing the clay content can lead to an enhancement in ionic osmotic pressure of hydrogels arising from the mobile ions on the nanoclay particles [32]. Secondly, nanoclay can act as a multifunctional crosslinker which subsequently limits the gel volume expansion [33]. Our results are in accord with the previous studies. Cyras et al reported that the water absorption rate decreased after introduction of MT into hydrogel composition [34]. Almasi et al also observed an improved water resistance in starch/carboxymethyl cellulose composite films by addition of the nanoclay, ascribing to the stronger hydrogen bonds between carboxylic groups of CMC and OH of

**Table 1.** Constant parameters for the swelling kinetic of CMC-g-Am/mMT hydrogels according to second order kinetic model.

	First order kinetic			Second order kinetic			$W_{\infty,exp}(g/g)$
	$k_1$ (min <sup>-1</sup> )	$W_{\infty 1}(g/g)$	$r^2$	$k_2$ (g g <sup>-1</sup> min <sup>-1</sup> )	$W_{\infty 1}(g/g)$	$r^2$	
<b>CMC-g-Am</b>	0.036	0.96	0.91	0.068	1.52	0.91	1.16
<b>CMC-g-Am/mMT1</b>	0.029	0.37	0.92	0.52	0.52	0.99	0.48
<b>CMC-g-Am/mMT2</b>	0.037	0.51	0.92	0.317	0.317	0.99	0.41

the MT layers [35]. Yin et al have proposed that the swelling kinetics of cross-linked hydrophilic hydrogels are compatible with the Schott's second-order diffusion models indicating that the swelling of hydrogels is controlled by stress relaxation of the network [36]. Accordingly, the experimental swelling data were analyzed by non-linear second-order swelling kinetic according to Schott's models described as Eq. 4 respectively [37].

$$W_t = \frac{k_2 W_e^2 t}{1 + W_e k_2 t} \quad (4)$$

Where,  $W_t$  is the water uptake at time  $t$ ;  $W_e^2$  is the theoretical equilibrium water uptake for second-order kinetic, and  $k_2$  is the specific rate constant for the second-order swelling kinetic. The coefficient of determination ( $r^2$ ) was utilized to evaluate the fitting of the experimental data by the second-order swelling model [38]. The model calculations were illustrated in Table 1. The value of  $r^2$  ( $\geq 0.98$ ) corroborated the well-fitting of data by second-order kinetic. Additionally, the calculated equilibrated water absorbency ( $W_e^2$ ) for hydrogels was close to the experimental equilibrium water absorbency ( $W_{e,meas}$ ) showing that the swelling rate is controlled by the stress relaxation in the network of hydrogel [39].

The swelling capability of prepared hydrogels was also studied in pH 1.2 and pH 7.4, corresponding to the pH of the stomach and colon respectively. As shown in Fig.4b the swelling ratios of hydrogels at pH 1.2 are lower than those of pH 7.4. It is due to the formation of hydrogen bond between -CONH- in the PAm chains, and -COOH in the CMC which promote polymer-polymer interactions over the polymer-water interactions, resulting in the decrement of swelling ratio [40].

### Controlled release of DS

#### Effect of pH

The accumulative releases profiles of DS from hydrogels were studied in both SIF and SGF simulated environments (Fig.5a-b). The release pattern of DS exhibited two separate regions: initial burst release in the first 30 min followed by a slower release up to 3 h. The rapid initial release was thought to be due to the dissolution and diffusion of the drug absorbed onto the surface of hydrogels. The second slower release phase was due to the higher density of cross-linked chains at hydrogel network which demotes diffusion of the drug entrapped within the inner part of the matrix [41]. In addition, DS-loaded hydrogels showed a more rapid release profile at pH 7.4 (intestinal fluid) compared to that of pH 1.2 (gastric media). In an acidic medium, the -COOH groups on the carboxy methyl cellulose backbone does not ionize and the gel structure is devoid of charge, therefore collapsing is observed because of hydrogen bonding formation (Fig.5b). Besides, it was partially attributed to the decreased solubility of DS at acidic pH [42]. The low solubility of DS at pH 1.2 is originated from the presence of weak carboxylic acid on the drug with pKa of about 4. At higher pH values (pH 7.4), carboxylic acid group converts to negatively charged carboxylate ions, accordingly electrostatic repulsion amongst the polymer chains, leads to more expansion of the network and increase in drug diffusion from the hydrogel. (Fig.5a). From the initial slope of release profiles, it can be concluded that the amount of drug released from hydrogels had good harmony with the swelling behavior of hydrogels. Besides, the rate and content of released drug were found to be slower in polymer/layered silicate hydrogel. According to the literature, the interaction between the sodium salt of Diclofenac and MT surface is

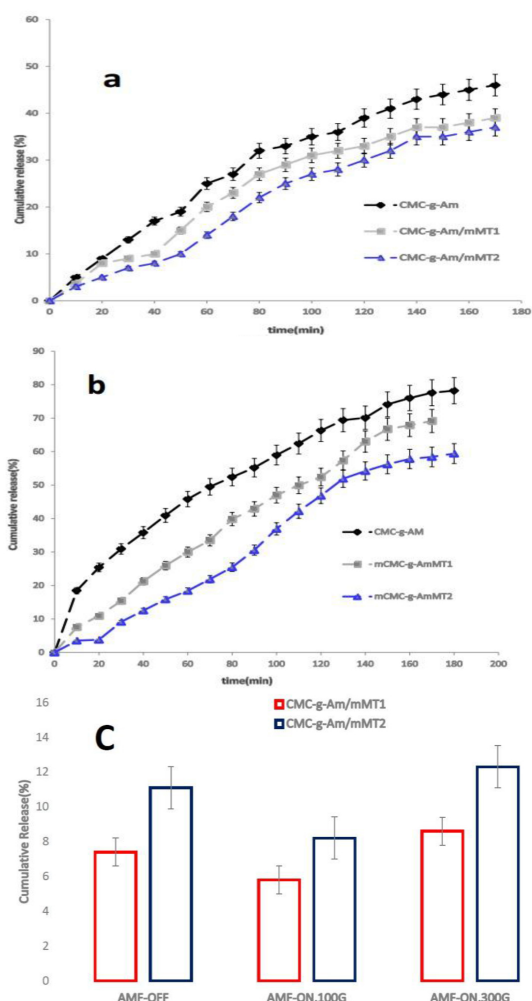


Fig. 5. Drug release profiles of nanocomposite hydrogels in a buffered solution with pH 7.4; (a) and pH 1.2 (b) (c) influence of external AMF on the drug release profiles of magnetic hydrogels at pH 7.4. (Mean ± 3, n=3)

stable enough to provide sustained release profile. As a consequence, the drug diffusion inside the matrix is controllable. Furthermore, MT offers nontoxic adsorption and mucoadhesive perspectives, which strongly encourage its application in drug-delivery systems compared to that of free-clay materials

[43].

Effect of external magnetic field

The release of DS from magnetic hydrogels was monitored as a function of field frequency (0, 100 and 300G) and concentration of the magnetic NPs shown in Fig. 5c. Concerning the effect of field frequency, we observed a higher release rate at high frequencies for increased MNPs concentrations. This increment in the amount of released drug under external magnetic field is referred to the alignment of magnetic nanoparticles with the applied AMF. To be specific more, the applied AMF can act as a stimulus to incite the magnetic nanoparticles which can increase the motion of magnetic nanoparticles leading to relaxation of polymer chains. The similar result was reported by Likhitkar et al. on controlled release of cisplatin from starch-based magnetic nanoparticles [44].

Mathematical modeling of release kinetics

The drug releases kinetic from hydrogels were estimated by using the Peppas model [45] expressed as Eq. 5:

$$\frac{M_t}{M_\infty} = kt^n \quad (5)$$

Where,  $M_t$  is the amount of drug released at time  $t$ , and  $M_\infty$  is total mass of drug loaded into the device,  $k$  is kinetic constant; and  $n$  is the release exponent. The parameters calculated by this model were summarized in Table 2. For  $n \sim 0.43$ , a Fickian diffusion and for  $0.43 < n < 0.85$ , a non-Fickian transport drug release mechanism dominates [46]. The  $n$  values were about 0.43 for magnetic clay- free hydrogel corresponding to Fickian diffusion. This observation is due to the high swelling degree of hydrogel and thereby highly network expansion. When a hydrogel network has a high degree of swelling its pore size becomes larger, hence the drug can be easily diffused into solution [46].

Table 2. Release parameters for drug release from CMC-g-Am/mMT hydrogels obtained after fitting the experimental data to the release kinetic models

Sample	$n$	$k \times 10^3$	$r^2$	Mechanism
CMC-g-Am	0.43	67	0.98	Non-Fickian
CMC-g-Am/mMT1	0.57	55	0.98	Non-Fickian
CMC-g-Am/mMT2	0.79	19	0.93	Non-Fickian

The  $n$  value was obtained  $>0.5$  for CMC-g-Am/mMT hydrogels indicating that the addition of mMT can shift the drug transport from Fickian mechanism to non-Fickian. The non-Fickian mechanism may be originated from the low swelling capacity of magnetic hydrogels referred to the more crosslinking points created by magnetic nanoparticles and nanoclay as multifunctional crosslinkers [47].

## CONCLUSIONS

In summary, we successfully manufactured pH-sensitive nanocomposite hydrogel based carboxymethyl cellulose-g-polyacrylamide/montmorillonite as a novel drug delivery system. The nanoscale hydrogels (CMC-g-Am/mMT) showed not only pH-dependent behavior but also a magnetic sensitivity to an external magnetic field, where the extents of drug released in basic solution was significantly higher than that of acidic media. Moreover, drug release rate can be tuned by operating the magnetic field. Notably, the findings shown in this work clearly highlights some outcome for the introduction of magnetic nanoclay into hydrogel structure. The mMT acted as a stabilizer to inhibit aggregation or further growth of magnetic iron oxide nanoparticles (MNPs). SEM results demonstrated that magnetic nanoclay (mMT) can cause a rough morphology. The swelling of nanocomposite hydrogel was affected by the content of magnetic nanoclay where introduction of nanoclay caused a significant reduction in swelling capacity from 20 g/g to 15 g/g.

## CONFLICTS OF INTEREST

The authors declare that there are no conflicts of interest regarding the publication of this manuscript.

## REFERENCE

1. Kozlovskaya V, Zavgorodnya O, Wang Y F, Ankner J, Kharlampieva E. Tailoring Architecture of Nanoscale Hydrogels: Effect of layering on pH-triggered swelling. *ACS Macro Lett.* 2013; (2):226–229.
2. Kozlovskaya V, Chen J, Tedjo C, Liang X, Campos-Gomez J, Oh J, Saeed M, Lunguc TC, Kharlampieva E. pH-Responsive Hydrogel Cubes for Release of Doxorubicin in Cancer Cells. *J. Mater. Chem. B.* 2014; (2): 2494-2507.
3. Kumar C S R, Mohammad F. Magnetic nanomaterials for hyperthermia-based therapy and controlled drug delivery. *Adv. Drug Delivery Rev.* 2011; (63): 789-808.
4. Mahdavinia GR, Etemadi H, Soleymani F. Magnetic/pH-responsive beads based on carboxymethyl chitosan and  $\kappa$ -carrageenan and controlled drug release. *Carbohydr Polym.* 2015; (128): 112-121.
5. Anderson SA, Rader RK, Westlin WF, Null C, Jackson D, Lanza C.M, Wickline SA, Kotyk, JJ. Magnetic resonance contrast enhancement of neovasculature with  $\alpha\beta$ 3-targeted nanoparticles. *Magn Reson Med.* 2000; 44 (3): 433–439.
6. Mahmoudi M, Sant S, Ben W, Laurent S, Tapas S. Superparamagnetic iron oxide nanoparticles (SPIONs): development, surface modification and applications in chemotherapy. *Adv. Drug Delivery Rev.* 2011; 63(1-2): 24 -46.
7. Zhang J, Misra R D K. Magnetic drug-targeting carrier encapsulated with thermosensitive smart polymer: core-shell nanoparticle carrier and drug release response. *Acta Biomater.* 2007; 3(6): 838-50.
8. Galbiati A, Tabolacci C, Morozzo B, Rocca D, Mattioli P, Beninati S, Paradossi G, Desideri A. Targeting Tumor Cells through Chitosan-Folate Modified Microcapsules Loaded with Camptothecin. *Bioconjugate Chem.* 2011; 22 (6): 1066–1072.
9. Hezaveh H, Muhamad I I. Controlled drug release via minimization of burst release in pH-response kappa-carrageenan/polyvinyl alcohol hydrogels. *Chem eng res des.* 2013; (91):508-519.
10. Choubey Y, Bajpai A. K. Investigation on magnetically controlled delivery of doxorubicin from superparamagnetic nanocarriers of gelatin crosslinked with genipin. *J Mater Sci: Mater Med.* 2010; (21): 51573–1586.
11. Zhu, K.; Yea, T.; Liua J, Peng Z, Xu S, Lei J H D, Li B. Nanogels fabricated by lysozyme and sodium carboxymethyl cellulose for 5-fluorouracil controlled release. *Int. J. Pharm.* 2013; 441(1): 721-727.
12. Lei H, Hongshan L, Liufeng L, Bin L. Green-step assembly of low density lipoprotein/sodium carboxymethyl cellulose nanogels for facile loading and pH-dependent release of doxorubicin. *Colloids Surf B Biointerfaces.* 2015; (126C): 288-296.
13. Butun S, Ince F G, Erdugan H, Sahinera N, One-step fabrication of biocompatible carboxymethyl cellulose polymeric particles for drug delivery systems. *Carbohydr Polym.* 2011; (86): 636–643.
14. Tas C, Ozkan C K, Savaser A, Ozkan Y, Tasdemir U, Altunay H. Nasal administration of metoclopramide from different dosage forms: in vitro, ex vivo, and in vivo evaluation. *Drug Deliv.* 2009; 16 (3): 167-75.
15. Anirudhan T S, Sandeep S, Divya P L. Synthesis and characterization of maleated cyclodextrin-grafted-silylated montmorillonite for the controlled release and colon specific

- delivery of tetracycline hydrochloride. *RSC Adv.* 2012; (2): 9555-9564.
16. Wen-fu L, Chen Y C. Superabsorbent polymeric materials. XII. Effect of montmorillonite on water absorbency for poly (sodium acrylate) and montmorillonite nanocomposite superabsorbents. *J. Appl. Polym. Sci.* 2004; 92(5): 3422-3429.
  17. Farshi Azhar F, Olad A A. study on sustained release formulations for oral delivery of 5-fluorouracil based on alginate-chitosan/montmorillonite nanocomposite systems. *Appl clay sci.* 2014; (101): 288-296.
  18. Depan D, Kumar A P, Singh R P, Cell proliferation and controlled drug release studies of nanohybrids based on chitosan-g-lactic acid and montmorillonite. *Acta Biomater.* 2009; 5 (1): 93-100.
  19. Lee YH, Kuo T F, Chen BY, Feng YK, Wen Y R, Lin W C, Lin F H. Toxicity assessment of montmorillonite as a drug carrier for pharmaceutical applications: yeast and rats model. *Biomed. Eng. Appl. Basis Commun.* 2005; 17(2): 12.
  20. Park J K, Choy Y B, Oh J M, Kim J Y, Hwang S J, Choy J H. Controlled release of donepezil intercalated in smectite clays. *Int. J. Pharm.* 2008; 359(1-2): 198-204.
  21. Lin FH, Lee YH, Jian C. H, Wong J. M, Shieh M J, Wang C Y A. study of purified montmorillonite intercalated with 5-fluorouracil as drug carrier, *Biomaterials.* 2002; 23(9): 1981-7.
  22. Zheng J P, Luan L, Wang H Y, Xi L F, Yao K D. Study on ibuprofen/montmorillonite intercalation composites as drug release system *Appl. Clay Sci.* 2007; 36(4): 297-301.
  23. Mahdavinia G R, Hasanpour S, Leila B, Sheykhloie Hossein. Study on adsorption of Cu(II) on magnetic starch-g-polyamidoxime/montmorillonite/Fe<sub>3</sub>O<sub>4</sub> nanocomposite hydrogels novel chelating ligands. *Starch/Starke.* 2016; 68 (3-4):188-199.
  24. Wu D, Zheng P, Chang P R, Ma X. Preparation and characterization of magnetic rectorite/iron oxide nanocomposite hydrogel and its application for the removal of the dyes. *Chem. Eng J.* 2011; 174 (1): 489-494.
  25. Mohapatra DK and Swagatika M. 5-Fluoro Uracil for colon specific drug delivery of a Poly (CarboxyMethyl Cellulose-co-Acryl Amide)/MBA Nano Sized Hydrogel. *IJCPS* 2012;1 (1) :250-262
  26. Zhang D, Karki AB, Rutman D, Young D P, Wang A, Cocke D, Ho T. H, Guo Z. Electrospun polyacrylonitrile nanocomposite fibers reinforced with Fe<sub>3</sub>O<sub>4</sub> nanoparticles: Fabrication and property analysis. *Polymers.* 2009; 50(17):4189-4198.
  27. Tzitzios V, Basina G, Bakandritsos A, Hadjipanayis C G, Mao H, Niarchos D, Tucek J, Zboril R. Immobilization of magnetic iron oxide nanoparticles on laponite discs-an easy way to incompatible ferrofluids and ferrogels. *J. Mater. Chem. B.* 2010; (20): 5418-5428.
  28. Xizian X, Fengzhu L, Yihe Z, Liling F. Synthesis and characterization of CPC modified magnetic MMT capable of using as anisotropic nanoparticles. *Chem. Eng J.* 2013; (216): 755-762.
  29. El-Di N. H. M, AbdAlla S. G, Wahab A, El-Naggar M. Swelling and drug release properties of acrylamide/carboxymethyl cellulose networks formed by gamma irradiation. *Radiat phys chem.* 2010;79(6):725-730.
  30. Kolhatkar A G, Jamison C A, Litvinov D, Willson C R, Lee T R. Tuning the Magnetic Properties of Nanoparticles. *Int J Mol Sci.* 2013; 14(8): 15977-16009.
  31. Omidian H, Park K, Kandalam U, Rocca J.G. Swelling and Mechanical Properties of Modified HEMA-based Superporous Hydrogels. *J. Bioact. Compat. Polym.* 2010; (25): 483-497.
  32. Li A, Zhang J, Wang A. Preparation and slow-release property of a poly (acrylic acid)/attapulgite/sodium humate superabsorbent composite. *J Appl Polym Sci* 2007; (103): 37 37-45.
  33. Darvishi Z, Kabiri K, Zohuriaan-Mehr M J, Morsali A. Nanocomposite super-swelling hydrogels with nanorod bentonite. *J Appl Polym Sci.* 2011; (120): 3453-3459.
  34. Cyrus V P, Manfredi L B, Ton-That M T, Vázquez A. Physical and mechanical properties of thermoplastic starch/montmorillonite nanocomposite films. *Carbohydr Polym.* 2008; (73): 55-63.
  35. Almasi H, Ghanbarzadeh B, Entezami A A. Physicochemical properties of starch-CMC-nanoclay biodegradable films. *Int. J. Biol. Macromolec.* 2010; (46): 1-5.
  36. Mistsumata T, Suemitsu Y, Fujii K, Fujii T, Taniguchi T. pH respond of chitosan, k-carrageenan and carboxymethyl cellulose sodium salt complex hydrogels. *Polymers.* 2003; 44(501): 7103-7111.
  37. Yin Y, Yang Y, Xu H. Swelling behavior of hydrogels for colon-site drug delivery. *J Appl Polym Sci.* 2002; (83): 2835-2842.
  38. Schott H. Swelling kinetics of polymers. *J macromol sci b.* 1992; (31): 1-9.
  39. Foo K Y, Hameed B H. Insights into the modeling of adsorption isotherm systems. *Chem. Eng J.* 2010; (156): 2-10.
  40. Zhang H, Zhai D, He Y. Graphene oxide/polyacrylamide/carboxymethyl cellulose sodium nanocomposite hydrogel with enhanced mechanical strength: preparation, characterization and the swelling behavior. *RSC Adv.* 2014; (4): 44600-44609.
  41. Xie M, Shi H, Ma K, Shen H, Li B, Shen S, Wang X, Jin, Y. Hybrid nanoparticles for drug delivery and bioimaging: Mesoporous silica nanoparticles functionalized with carboxyl groups and a near-infrared fluorescent dye. *J. Colloid Interface Sci.* 2013; (395): 306-314.

42. Hu S H, Liu T Y, Huang H Y, Liu D M, Chen S Y. Magnetic-sensitive silica nanospheres for controlled drug release. *Langmuir*. 2008; (24): 239-244.
43. Cypes S H, Saltzman W M, Giannelis E P. Organosilicate-polymer drug delivery systems: controlled release and enhanced mechanical properties. *J. Control. Release*. 2008; 90(2):163-9.
44. Likhitar S, Bajpai A K. Magnetically controlled release of cisplatin from superparamagnetic starch nanoparticles. *Carbohydr Polym*. 2012; (87): 300-308.
45. Siepmann, J.; Peppas, N. A.: Modeling of drug release from delivery systems based on hydroxypropyl methylcellulose (HPMC). *Adv. Drug Delivery Rev*. 2001; (48): 139-157.
46. Bardajee G R, Hooshyar Z, Asli M J, Shahidi F E, Dianatnejad N. Synthesis of a novel supermagnetic iron oxide nanocomposite hydrogel based on graft copolymerization of poly ((2-dimethylamino) ethyl methacrylate) onto salep for controlled release of drug. *Mater Sci Eng C*. 2014; (36): 277-286.
47. Soppiranth K S, Aminabhavi TM. Water transport and drug release study from cross- linked polyacrylamide grafted guar gum hydrogel microspheres for the controlled release application. *Eur. J. Pharm. Biopharm*. 2002; (53):87-98.